Statistical Damage Diagnosis in Smart Systems Using Non-Contact Magnetoelastic MetGlas Sensors and Stochastic Modeling of System Output Data

Dimitrios G. Dimogianopoulos
Stochastic Mechanical Systems & Automation (SMSA) Group,
Department of Mechanical and Aeronautical Engineering, University of Patras, GR 26504, Greece
dimogian@mech.upatras.gr
Dionysios E. Mouzakis
Department of Materials Science, University of Patras, GR 26504, Greece
mouzakis@upatras.gr
Dimitrios Kouzoudis
Department of Engineering, University of Patras, GR 26504, Greece
kouzoudi@upatras.gr

Abstract- ***This study introduces a non-destructive/contact-free methodology, which utilizes Magneto-Elastic (ME) Metallic Glass (MetGlas) stripes in order to evaluate the mechanical response of vibrating polymer slabs and achieve statistical diagnosis (that is, detection and severity evaluation) of damage. The magnetization of ME materials is linked to their mechanical properties, that is, remote (contact-free) magnetic measurements can reveal information on the internal state of the material. Such ME MetGlas alloy stripes are attached to polymer epoxy resin slabs, and the resulting smart systems are dynamically loaded at time–related, growing oscillation amplitudes in a TA Instruments Dynamic Mechanical Analyzer. Both "healthy" and "damaged" (faulty) systems are tested, with the inflicted damage being a number of sequentially drilled holes of given diameter (at each test run an extra hole is created). The system's response to the DMA excitation is remotely collected (contact-free) via a coil located over the slab. Such signal data (in mV) obtained from a benchmark healthy system, are modeled via advanced stochastic output-only Nonlinear AutoRegressive (NAR) representations, in order to code the healthy system dynamics. Ultimately, diagnosis of potential damage, for a system in unknown health state, is reliably achieved by collecting its test data, and statistically comparing its dynamics with those of the (NAR modeled) benchmark healthy system***.

Keywords: Contact-free measurements, statistical damage diagnosis, nonlinear modeling, MetGlas

1 Introduction

Certain materials are able of expanding or shrinking when exposed to an applied magnetic field, with typical internal strains of the order of 0.1%. This key property, referred to as magneto-elasticity, applies also in the opposite sense: When a certain amount of stress is applied to these materials, their magnetic properties change [1]. Because of these two characteristics, Magneto-Elastic (ME) materials find many uses like sensors, actuators, pumps, high force linear motors, ultrasonic cleaners, and sonar. The two most common ME materials, Terfenol-D and MetGlas have become commercially available in the mid to late 1980s. MetGlas is produced by Allied Signals in thin ribbon forms by continuous rapid quenching of the melt, and is well suited to various applications because it is metallic, cheap and amorphous. Due to the significant potential applications of MetGlas alloys, numerous publications on their characterization (mechanical, magnetic, and material properties) have emerged. In a review article on applications of metallic glasses, Hernando et al. [2] mention that metallic glasses are by far the best-known materials for mechanical stress sensing because of their high sensitivity of 10^5 and their good temperature stability. Further advantages include the outstanding elastic and magnetic properties, the high atomic mobility, the high homogeneity, and the absence of grain boundaries, dislocations, and similar defects. Hristoforou [3] gives a review article on the use of ME materials in delay lines for sensing applications, while Arcas et al. [4] measure a typical property (hysteresis loop) and deduce the stress distribution of a plastic strip with a metallic glass ribbon attached to it.

Obviously, measuring the aforementioned properties may also help to conclude on the health state of a given system, when its material and structural properties are already known: The system response data collected by means of MetGlas alloys may constitute a valuable yet inexpensive way of assessing its health state, based upon the principle that small structural changes cause modifications of the system properties, which affect the system response signals [5],[6]. As a result, reliable statistical detection of potential system damage and evaluation of its severity can be achieved. Over the last few years, this principle along with conventionally collected data (through normal sensors) has led to particularly promising statistical diagnosis approaches and applications (see [7] and the references therein). Potential advantages of such approaches include inherent accounting for (measurement, environmental, modeling and so on) uncertainty due to the use of statistical tools, and capability of working at a "system" level. Furthermore, these approaches tend to be time effective and less expensive than most alternatives.

The current study aims at utilizing promising ME MetGlas stripes to evaluate the mechanical response of vibrating

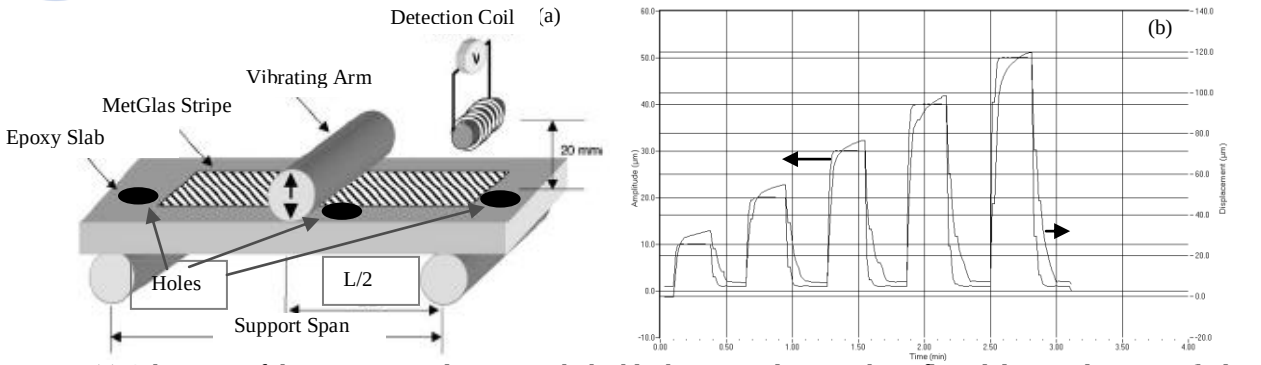

Figure 1: (a) Schematic of the experimental set up with the black spots indicating the inflicted damage locations (holes of diameter equal to 2.25mm); (b) DMA dynamic loading chart with the vibration amplitude (left *y*-axis) and the slab response (displacement, right *y*-axis) versus time.

polymer slabs and statistically conclude on their health state by means of a contact-free and non-destructive approach. Specifically, the (30μm thin) 2826MB MetGlas stripes are used as embedded elements in polymer slabs, thus forming smart systems whose mechanical behavior and current health state are assessed, and occurring damage is diagnosed (that is, detected and its severity evaluated). The experiment procedure involves a polymer epoxy resin slab with a stripe of ME MetGlas alloy attached to its surface. This smart system is tested in both "healthy" and "faulty" states (that is, state involving damage of various levels). The artificial damage is inflicted by sequentially drilling a number of holes of given diameter on the slab (one extra hole at each test). Both healthy and faulty systems are dynamically loaded under one or more frequencies in time–related growing oscillation amplitudes in a TA Instruments Dynamic Mechanical Analyzer (DMA). Displacements as low as 20 μm may be measured with a gauge factor equal to 11,700 [1]. The system's response to the DMA excitation is remotely collected (contact-free) via a coil located over the slab.

As stated previously, dynamically loading the smart system produces an output signal depending upon (and including information on) the structural properties of the system in its current health state [8]. This output signal (along with the inherent health state information) may be modeled via suitably selected output-only stochastic Nonlinear AutoRegressive (NAR) representations [9], which (being of stochastic nature) are able to account for noise and other disturbance-related uncertainties in the measured data. The key idea of the proposed diagnosis approach lies on the benchmark healthy system's dynamics (that is, the dynamic behavior resulting from its structural properties) being accurately modeled via NAR representations identified on system output data. Ultimately, diagnosis of potential damage for a similar system in unknown health state is reliably achieved by collecting its test output data, and statistically comparing its dynamics with that of the benchmark (NAR-modeled) healthy system.

2 The Experimental Setup and Testing Procedure

The experimental set-up consists of (a) the smart system (epoxy slab and attached MetGlas stripe), (b) the dynamic mechanical analysis (DMA) tester, and (c) the detection device. The smart system is an epoxy resin slab (LTM 217 Advanced Composites Group Ltd., Derbyshire, UK) of dimensions 50mm×14.63mm×2.31mm, with a MetGlas 2826MB stripe measuring 40mm×6mm×30μm (with average composition Fe40Ni38Mo4B18) attached to its surface using cyanoacrylate glue. The DMA tester Q800 of TA instruments is used for the dynamic strain tests. Usually, such instruments are used to determine the viscoelastic behavior of materials by applying a sinusoidal stress (0.01–200Hz) and/or heat (0.1–60 °C/min) while monitoring the force and the deflection (typically a few micrometers). The technique can be adapted for almost any type of sample including gels and powders. In the present case, all measurements are performed at room temperature and the signal of interest is the strain of the epoxy resin slab. The DMA is operated in three point bending mode, that is, the system is supported at three points, two of which are fixed and the third one is driven by a linear actuator at the prescribed frequency [see Fig. 1(a)]. The detection mechanism consists of a 28 gauge copper coil with induction of 6.6H and resistance of 1700Ω, placed at 2 cm over the system. The coil is connected to a custom-made preamplifier with a gain equal to 20, which drives the output signal (in mV) via a RS 232 interface to a Pentium®4 PC, where it is sampled at 44100Hz and stored.

Loading frequencies may be set at various frequencies up to 200Hz. In the current case, the system was subjected to vibration at 150Hz by a sinusoidal stress with the amplitude profile being set to five main levels of 10, 20, 30, 40, and 50μm, as shown in Fig. 1(b) (left *y*-axis). In order to clearly delimit the system's output response, the system vibrates at ultra low amplitude (1μm) both before and after each change of amplitude level. Hence, the final amplitude level sequence is 1-10-1-20-1-30-1-40-50-1μm. The curve evolution in Fig. 1(b) for t < 0.50 min is part of the DMA instrument's report. Also shown in the same figure, is the system's bending displacement (right *y*-axis), which is basically the system (slab plus MetGlas stripe) response to the applied bending amplitude imposed by the oscillating DMA arm. Note that a static load of 0.01N is applied before each test, in order to ensure perfect contact between the arm and the slab at all times. The series of test runs involve systems in healthy state or with various levels of inflicted damage. The considered damage corresponds to a number of holes (of a diameter equal to 2.25mm) sequentially drilled onto the slab (one extra hole at each run). Special care is taken to avoid drilling holes symmetrically to any major slab axis. Finally, an additional test is specifically designed for estimating the influence of noise due to the coil, the cables

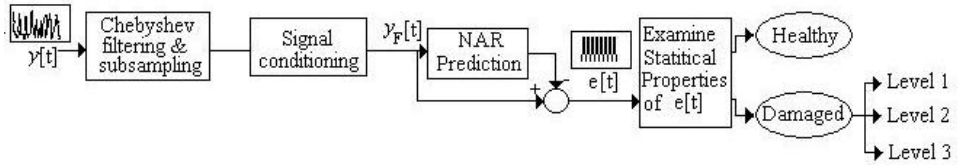

Figure 2: Operational principle of the damage diagnosis scheme

Table 1: The vibration test runs performed

Test run number	System health state	DMA excitation frequency (Hz)	System output sampling frequency (Hz)	Total test run duration (min)
1	Healthy	0	44100	3.09
2	Healthy	150	44100	3.25
3	One hole	150	44100	3.25
4	Two holes	150	44100	3.25
5	Three holes	150	44100	3.25

and other parts of the experimental set up. This test involves recording the coil output (which corresponds to the system response) without the DMA arm oscillating. As shown in section 3.1, this signal provides valuable information for the definition of the system response frequency range which may be examined for diagnosis purposes. The various tests performed are presented in Table 1.

3 The Damage Diagnosis Procedure

The damage diagnosis procedure involves two phases. During the first phase, referred to as the data modeling phase, part of the benchmark healthy system dynamics (that is, a selected frequency range of the system output) is conditioned and modeled via NAR representations. This choice of frequency range depends on the noise corrupting the system output measurements and is discussed during the detailed presentation of the first phase in section 3.1.

During the second phase, referred to as the assessment phase, the dynamics of a similar system in unknown health state are compared to those corresponding to the benchmark (NAR-modeled) healthy system. For a healthy system under inspection, the NAR provided one-step-ahead prediction of the system output (see Fig. 2) is statistically similar to the corresponding test-obtained signal. For a damaged system, however, the difference between the NAR-predicted and the actual signal (the residual $e[t]$ in Fig. 2) will however change, thus reflecting the change in the health state of the system. Then, the damage-related information is extracted from $e[t]$ through evaluation of its statistical properties and damage diagnosis is statistically concluded. The assessment phase is presented in detail in section 3.2.

3.1 Data Modeling Phase

For a system in healthy state, the output-only representation relating the current output value to older ones has the form:

$$y[t] = \sum_{i=0}^{L} \theta_i[t] \cdot p_i[t] + e[t]$$
$$e[t] \sim NID\ 0, \sigma_e^2 \qquad (1)$$

with t designating the normalized discrete time, and $y[t]$, $e[t]$ the output and one-step-ahead prediction error [or residual, assumed to be a zero-mean uncorrelated sequence with variance σ_e^2] signals, respectively. NID $\sim$ stands for Normally Independently Distributed (with the indicated mean and variance). The maximum lags of the output signal $y[t]$ in (1), referred to as model order, is n_y. The nonlinear terms $p_i[t]$ are referred to as regressors, and are products between output signal data values (ranging from $y[t-1]$ up to $y[t-n_y]$). The nonlinearity degree of the representation is denoted as *nl* (that is, the sum of powers of the signal values involved in each regressor is less than or equal to *nl*). The *i*-th regressor coefficient (parameter) is noted θ_i and is time invariant.

During the data modeling phase the objective is to identify the NAR representation, that is: (a) To choose the regressors $p_i[t]$ that most accurately describe the system dynamics, and (b) to estimate the associated parameters θ_i. For this purpose, the top equation in (1) is rewritten as[1]:

$$y[t] = \boldsymbol{\varphi}^T[t] \cdot \boldsymbol{\theta} + e[t] \qquad (2)$$

with $\boldsymbol{\varphi}[t] = \begin{bmatrix} p_0[t] & \dots & p_L[t] \end{bmatrix}^T$ and $\boldsymbol{\theta} = \begin{bmatrix} \theta_0 & \dots & \theta_L \end{bmatrix}^T$ the parameter vector. The total test run data (N samples) may then be represented by a matrix equation as follows:

$$\boldsymbol{y} = \boldsymbol{\Phi} \cdot \boldsymbol{\theta} + \boldsymbol{e} \qquad (3)$$

[1] Lower case/capital bold symbols designate column vector/matrix quantities, respectively.

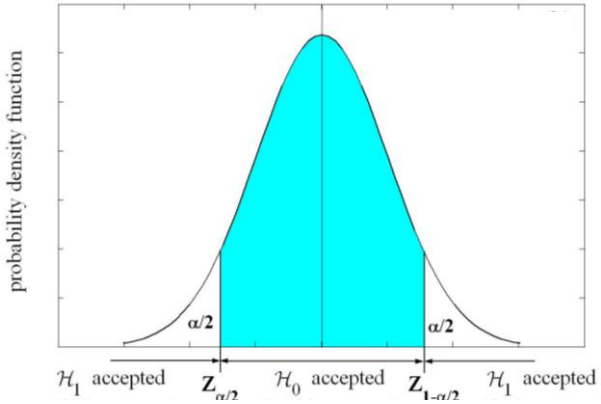

Figure 3: Statistical hypothesis test for checking normality of the correlation coefficient ρ_i of the sequence $e[t]$ (the shaded area corresponds to accepting H_0 at risk level α)

with $\boldsymbol{y} = [y[1] \ldots y[N]]^T \in \Re^{N\times 1}$, $\boldsymbol{e} = [e[1] \ldots e[N]]^T \in \Re^{N\times 1}$ and $\boldsymbol{\Phi} = [\boldsymbol{\varphi}[1] \ldots \boldsymbol{\varphi}[N]]^T \in \Re^{N\times(L+1)}$. The selection of p_i is made by means of a Forward Orthogonal Search (FOS) algorithm [10]. Briefly, an initial set of potential regressors containing all possible product combinations (of nonlinearity degree up to *nl*) formed by the output signal values $[y[t\text{-}1] \ldots y[t\text{-}n_y]]$, is considered. The selection procedure is iterative and starts by searching the most significant regressor term, defined by its contribution to the reduction of the Residual Sum of Squares to the modeled Signal's Sum of Squares (RSS/SSS) ratio (the RSS being computed from the $e[t]$ sequence and the SSS from the modeled system output signal). The term leading to the largest RSS/SSS reduction at each iteration is stored, and the next most significant one is sought until a user-defined number of regressors is selected. When the desired number of p_i terms has been selected, the vector $\boldsymbol{\theta}$ is estimated by using (3) and an Ordinary Least Squares (OLS) or a Weighted Least Squares (WLS) algorithm ([11] pp. 676-679). The FOS algorithm performs efficient regressor selection for a given signal, with its principal merit being that regressors are selected upon their importance: Those leading to bigger RSS/SSS reductions are selected first. Hence, *model reduction* (that is, the procedure reducing an accurate but with numerous terms NAR representation to an equally well performing but "shorter" one) is easily performed as will be shown in section 4.1.

Typically, the identified NAR representation is validated by checking the correlation of the obtained residual $e[t]$, and the RSS/SSS ratio. The identified representation is statistically adequate if the RSS/SSS values are low ($< 10^{-2}$) and the residual sequence is uncorrelated. This last point is checked by means of the autocorrelation coefficients ρ_i (see [12] p.26) at lag i of the residuals, which reflect the dependency (or correlation) between the $e[t]$ and the $e[t\text{-}i]$ values. Obviously, the values ρ_i of an uncorrelated sequence are statistically close to zero, for all lags i=1...l. Each coefficient ρ_i of the sequence follows normal distribution with zero mean and variance equal to $1/N$ ([12] p. 34), with N being the number of sequence data samples. Given that a statistically adequate modeling of the system dynamics leads to uncorrelated residuals, a composite hypothesis test based on ρ_i (and executed $\forall$ i=1,...l) is constructed as follows:

$$\begin{aligned} H_0: &\quad \rho_i = 0 \quad \text{(adequate system representation)} \\ H_1: &\quad \rho_i \neq 0 \quad \text{(inadequate system representation)} \end{aligned} \tag{4}$$

with H_0 and H_1 designating the null and alternative hypothesis, respectively. From basic properties of the normal distribution, the quantity ρ_i normalized by its standard deviation follows normal distribution with zero mean and variance equal to 1, that is $\rho_i / (1/\sqrt{N}) = \sqrt{N}\rho_i \sim \mathcal{N}(0,1)$. Hence, if $Z = \sqrt{N}\rho_i$ is defined, the following hypothesis test at the risk level α (that is, the probability of rejecting H_0 given that H_0 is true) is formed:

$$\begin{aligned} Z_{\frac{a}{2}} \le Z \le Z_{1-\frac{a}{2}} \quad or \quad \frac{1}{\sqrt{N}} Z_{\frac{a}{2}} \le \rho_i \le \frac{1}{\sqrt{N}} Z_{1-\frac{a}{2}} \quad &\Rightarrow \quad H_0 \text{ is accepted} \\ \text{Else} \qquad\qquad\qquad\qquad\qquad\qquad\quad &\Rightarrow \quad H_1 \text{ is accepted} \end{aligned} \tag{5}$$

with Z_a the standard normal distribution's α critical point (see Fig. 3). Uusually, the true but unknown ρ_i is replaced by its estimated value $\hat{\rho}_i$ (see [13], p. 424), which is trivially computed in various software packages like MATLAB™. The values $\hat{\rho}_i$ for various lags are then plotted on a single chart along with the statistical upper and lower limits at the given risk level α [the inequality bounds in (5)], which are valid when the sequence is uncorrelated. If the large majority of $\hat{\rho}_i$ values is located in-between these limits, the H_0 hypothesis is accepted at the given risk level α. Typically, the values $\hat{\rho}_i$ of the 30-50 initial lags are critical for checking the lack of correlation of $e[t]$ sequence, and are systematically examined. The validation of the NAR representation in the current study is described in section 4.1.

An important issue of the data modeling phase is the proper output signal preparation (mainly by filtering a range of frequencies) before its modeling. As mentioned before, the coil-provided system output measurements [see Fig.1(a)] are corrupted by noise, due to the coil itself and the measuring devices. Hence, much of the output signal's frequency content is masked by colored noise, and only the remaining part of it may be used for diagnosis purposes. The selected

signal frequency range to be modeled has a significant effect on the effectiveness of the damage diagnosis procedure and is presented in detail in section 4.1.

3.2 Assessment Phase

The signal $e[t]$ is used for damage diagnosis (that is, detection and severity evaluation) purposes, as shown in Fig.2. The detection part is based upon the lack of correlation property of the $e[t]$ sequence, as obtained when a system in healthy state is tested. In the case of a fault-affected/damaged system, the signal $e[t]$ will be correlated and this can be checked by means of another composite hypothesis test for the correlation coefficient ρ_i at lag i:

$$\begin{aligned} H_0: &\quad \rho_i = 0 \qquad \text{(healthy system)} \\ H_1: &\quad \rho_i \neq 0 \quad \text{(faulty/damaged system)} \end{aligned} \tag{6}$$

with H_0 and H_1 designating the null and alternative hypothesis, respectively. The test is implemented as that shown in section 3.1 for the system modeling validation task: Given that each autocorrelation coefficient follows normal distribution with zero mean and variance equal to $1/N$, the quantity $Z^* = \sqrt{N}\rho_i$ is defined, the unknown ρ_i is replaced by $\hat{\rho}_i$ with statistical limits at the risk level α established as in (5), and autocorrelation plots may be formed. However, as opposed to the procedure in section 3.1, the test may be performed on even a *single* autocorrelation coefficient.

The damage severity evaluation part is a more complicated task. In the current study, the damage inflicted on the slab consists of sequentially drilled holes (one extra hole created at each test), as presented in Table 1 and Fig. 1(a). Consequently, the damage grows along with the number of holes, and this should be reflected in the results. Hence, for a given group of test runs, with each run corresponding to a system affected by a different level of damage, a clear classification between the most and the less damaged systems should be established through a suitably selected metric.

Given that the autocorrelation coefficients are computed for the damage detection part, it would be desirable to use a selected group of them to define a metric and perform severity evaluation, as well. After extensive tests, it results that the damage level may indeed be related to specific correlation coefficient estimates through the quantity (metric) Q:

$$Q = \left|\hat{\rho}_1 + \hat{\rho}_2\right| \tag{7}$$

with $\hat{\rho}_1$ and $\hat{\rho}_2$ the estimated autocorrelation coefficients at lag 1 and 2, respectively. For the given system, with holes drilled in the locations shown in Fig. 1(a), the metric Q grows simultaneously with increasing damage, at least for the majority of considered cases, as shown in section 4.2, where the damage diagnosis results are presented in detail. Note that this selection of coefficients for damage severity evaluation is by no means unique, and depends (among others) upon the identified NAR representation, the initial filtering and conditioning of the output signal and so on.

4 Damage Diagnosis Results

As mentioned in section 2, five test runs are conducted. The duration of each test run is 3.25mins (except for test run 1) and data are recorded at 44100Hz. The test run 1 is performed in order to estimate the noise levels in the system output measurements. The data set of test run 2 is separated into two parts, namely the identification (from 0.2 to 2.45mins) and the assessment (from 2.45 to 3.1mins) parts. The first part starts at 0.2min to avoid any transient phenomena due to the DMA calibration and is solely used to identify the NAR representation for the healthy system (see section 3.1). The second part is used for obtaining diagnosis results, meaning (for the considered test run 2) to check and validate that the system is in healthy state. The signal part after 3.1mins is not used, since it corresponds to low amplitude DMA excitation. Finally, for test runs 3-5, the signal part from 0.2 to 3.1mins is used for obtaining damage diagnosis results.

4.1 Data Modeling Results

The data modeling results are obtained from test run 2 (see Table 1), where testing of the healthy system is performed. An initial consideration is related to the noise levels in the system output data. This noise masks any potential information related to the system health state and must, therefore, be filtered. For this purpose, the power spectral density for both the noise (test run 1) and the healthy system output data (test run 2) are drawn in a single figure and shown in Fig. 4(a). Through careful examination of Fig. 4(a), significant output frequency components are *clearly* distinguished over the noise *only* for a limited number of frequencies. This is also verified in Fig. 4(b), where obviously a major part of the system's measured output is corrupted by noise, especially at the end of the test run, that is, during the period of large amplitude vibrations (see section 2). Two such frequency regions are shown in detail in Fig. 4(a): The frequency range around 153Hz (which is reasonable given the DMA arm oscillating at 150Hz) and its harmonic at approximately 460 Hz. At both frequency ranges the system's output data spectral magnitude is at least 20-40 db larger than that of the noise. Hence, a Chebyshev II band-pass filter (whose characteristics are shown in Table 2) is designed to only retain the frequency range around 153Hz. Subsequently, the output data y (originally sampled at 44100Hz as shown in Table 1) are resampled at 441Hz. Note that the frequency range around 153Hz is preferred to that around 460Hz for practical reasons: Indeed, had this last been selected, the signal y should have been resampled at a frequency close to 1000Hz, which would lead to a filtered signal with twice as much samples compared with the current one.

Another issue comes with the remaining noise after the signal filtering around 153Hz. As seen in Fig. 4(c), the filtered signal (in red) still contains colored noise components, although of very small magnitude. However, the effect of this

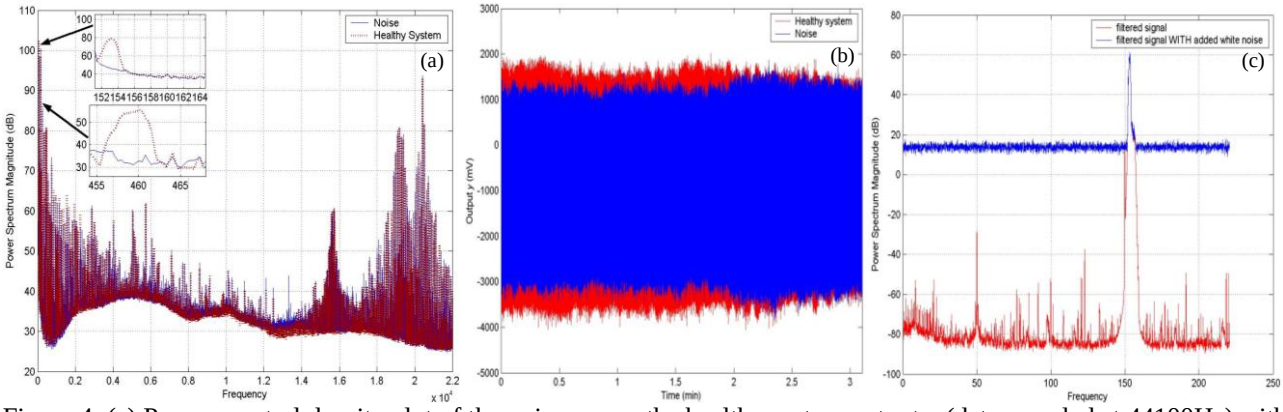

Figure 4: (a) Power spectral density plot of the noise versus the healthy system output y (data sampled at 44100Hz) with selected frequencies in detail; (b) Plot of noise versus healthy system output y (data sampled at 44100Hz); (c) Power spectral density plot of the (filtered around 153 Hz) system output signal and the same after conditioning.

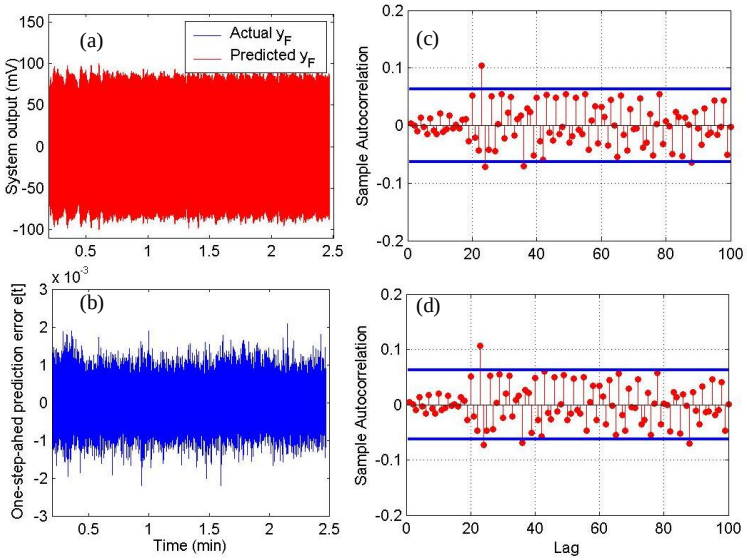

Figure 5: (a) Actual signal y_F versus its one-step-ahead prediction from the first stage NAR(25) representation; (b) one-step-ahead prediction error $e[t]$ from NAR(25) representation; (c) autocorrelation plot of $e[t]$ for validation of the NAR(25) representation before the reduction procedure; (d) autocorrelation plot of $e[t]$ for validation of the NAR(25) representation after the reduction procedure (horizontal lines designate statistical limits at the $\alpha=10^{-5}$ risk level)

Table2: Characteristics of the initial data filter (Chebyshev II) and the identified NAR(25) representation

Number of regressors (linear/nonlinear)	RSS/SSS	Identification time in hrs (Pentium 4, 3GHz)
200 (25/175) before reduction	0.0084	6.8 *
70 (25/45) after reduction	0.0086	1.5 **

* Regressor selection and parameter estimation time, ** Cumulative parameter estimation time for all steps

Chebyshev II band-pass filter used for initial filtering of system output data (designed in MATLAB© v. 6.5)

Initial sampling frequency of system output: Fs=44100Hz				Band-pass frequency area: 152-156Hz			
Lower frequency area border				Upper frequency area border			
Fstop1 (lower cut) =149Hz	at	Astop1=120	db	Fpass2 (lower pass)=156Hz	at	Apass= 1	db
Fpass1 (higher cut)=152Hz	at	Apass = 1	db	Fstop2 (cutoff at) = 160Hz	at	Astop2= 80	db

noise is important to the extent that the identified NAR representation will also model the noise part in the signal. This complicates the NAR representation by adding extra (noise accounting) terms, which are obviously undesirable. For this purpose, the filtered signal is conditioned by adding a white noise layer (with standard deviation σ=5, in the present case) in order to cover these undesirable noise components. As shown in Fig. 4(c) (in blue), the final signal, referred to as y_F now contains only the frequency range around 153 Hz with the other frequency parts corresponding to *almost* white noise (since it includes some insignificant colored noise components), which, by definition, can not be modeled.

A NAR(25) representation (that is, n_y=25) involving 200 regressors with nonlinearity degree nl=2 is identified. Its characteristics are shown in Table 2. Typical results are given in Fig. 5(a), (b), where the one-step-ahead predictions and the prediction error for the identified NAR(25) representation are respectively shown. The one-step-ahead prediction of the y_F is remarkable, as highlighted by the low corresponding RSS/SSS value in Table 2. As shown in

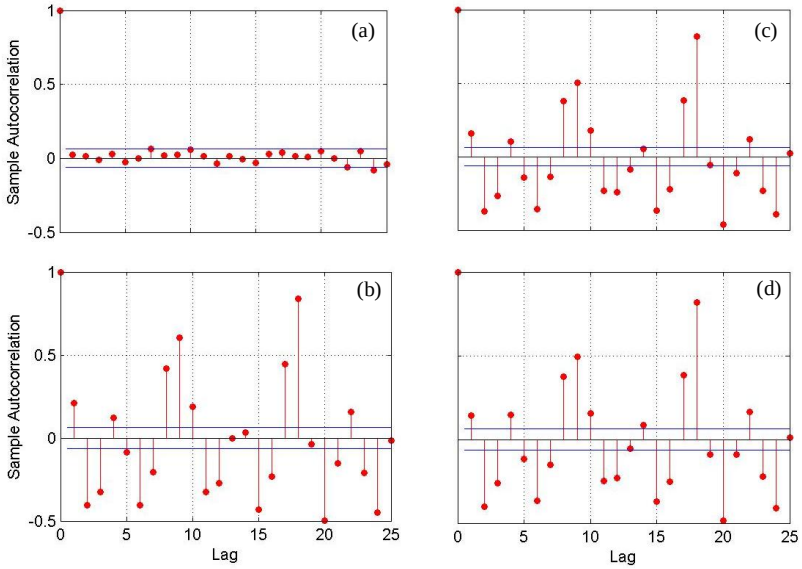

Figure 6: Autocorrelation coefficients of residuals $e[t]$ from test runs with system (a) in healthy state, (b) with one hole, (c) with two holes and (d) with three holes (horizontal lines designate statistical limits at the α=10^{-5} risk level)

Fig.5(c), the NAR(25) residuals are almost uncorrelated. The relevant results of Table 2 are obtained from the test run 2 part from 2.46 to 2.64mins [that is, the signal part not used in the NAR(25) identification].

Remark: Generally, for off-line damage diagnosis applications, minimizing the number of regressors is not always a priority: Large regressors sets mainly lead to extra time dedicated to the identification of the NAR representation. However, in the damage diagnosis phase (section 4.2), the results (involving the computation of $e[t]$ sequence via predictions from the identified NAR representation) are almost instantaneous. Nevertheless, the current NAR(25) representation contains a significant amount of terms and could greatly benefit from a model reduction procedure. As mentioned in section 3.1, this is relatively easy with the FOS algorithm, because the regressors are selected upon their importance. Hence, for reducing the total number of terms, the lastly selected regressors are sequentially omitted (one at a time), parameter estimation is again performed and the newly obtained residuals $e[t]$ are inspected with respect to their correlation and the RSS/SSS ratio. The results of this procedure in the current case are given in Table 2: The total number of regressors has been drastically reduced to 70, the RSS/SSS ratio has only slightly increased, and the autocorrelation plot for the reduced representation in Fig. 5(d) is almost identical to that of the initial one in Fig. 5(c).

4.2 Assessment Results

The assessment phase involves two parts, namely damage detection and severity evaluation. Damage detection is performed using the lack of correlation property of the sequence $e[t]$, checked by means of the composite test (6) and the statistical quantity Z^* (see section 3.2). The estimated autocorrelation coefficients $\hat{\rho}_i$ for lags i=1,...,25 are computed along with their statistical limits [given in (5)], and shown in Fig. 6 for test runs conducted with systems at various health states. The horizontal lines designate the statistical limits for $\hat{\rho}_i$ [the lower and upper bound in the inequality (5)] at the α=10^{-5} risk level. Figure 6(a) shows the values of $\hat{\rho}_i$ with i=1,...,25, for test data obtained from a healthy system (test run 2). As stated in section 3.2, performing the composite test on one (properly selected) lag permits to conclude on the health state of the system. In this case, choosing the proper lag is trivial since the estimated correlation coefficients for *almost all* lags shown are in-between the statistical limits. This means that performing the composite test on any of the aforementioned lags leads to the hypothesis H_0 (system in healthy state) being accepted at the α=10^{-5} risk level. Figures 6(b), (c) and (d) show the values of $\hat{\rho}_i$ with i=1,...,25, for data obtained from a system with one (test run 3), two (test run 4) and three holes (test run 5), respectively. Now, the estimated correlation coefficients for *almost all* lags lie off the zone denoted by the statistical limits. Hence, performing the composite test on any of the aforementioned lags leads to the hypothesis H_0 (system in healthy state) being rejected in favour of the alternative H_1 (faulty/damaged system) at the α=10^{-5} risk level. Note that these typical results correspond to the part from t=2.65 to t=2.84mins of the test runs 2-5. This means that in Fig. 6(a) conclusions are drawn from the signal part of test run 2, which corresponds to large amplitude oscillations and has not been used for identifying the NAR(25) representation. The composite test has been applied to various parts of the signals obtained from test runs 2-5 and the corresponding results are shown in Table 3. All systems tested in damaged state for a given signal part (that is, given amplitude oscillation) are correctly detected as such. This is due to the identified multi-stage NAR(25) representation, which models accurately the entire healthy system dynamics. Hence, even the slightest effect of damage on the system dynamics can be easily detected.

Furthermore, the damage severity is also evaluated by means of the metric (7). It is also easily seen that in all but one cases, the level of damage inflicted to the system is correctly estimated, with the quantity Q growing with increasing

Table 3: Damage diagnosis results for test runs 2-5 corresponding to various system health states (wrong damage severity evaluation is indicated by "•")

Signal part used for damage diagnosis	Test run 2 (healthy)		Test run 3 (1 hole)		Test run 4 (2 holes)		Test run 5 (3 holes)	
	Detection	Q	Detection	Q	Detection	Q	Detection	Q
From 0.2 to 2.45 min	healthy	0.0009	YES	0.1753	YES	0.1890	YES	0.2190
From 2.46 to 2.64min	healthy	0.0046	YES	0.1663	YES	0.1997	YES	0.2284
From 2.65 to 2.84min	healthy	0.0414	YES	0.1935	YES	0.2144	YES	0.2567
From 2.85 to 3.03min	healthy	0.0112	YES	0.2016	YES	0.1669•	YES	0.2350

damage. Even for the one missed case (that corresponding to signal parts from 2.85 to 3.03min), the damage level corresponding to three holes is correctly picked up, and only the two other damage levels are estimated in the wrong order. The location of the second hole [towards the slab border close to the vibrating DMA arm, see Fig. 1(a)] may probably be related to this result, since the two other holes are almost equally offset with respect to the DMA arm.

5 Conclusions

This work introduced a novel non-destructive/contact-free approach to perform statistical diagnosis (that is, detection and severity evaluation) of damage through vibration testing. MetGlas stripes were attached to polymer slabs, thus forming smart systems which were dynamically loaded at time–related, growing oscillation amplitudes in a DMA tester. The system output data in healthy state were collected in a contact-free manner, and utilized along with NAR representations to model the healthy system's dynamics. Subsequently, the dynamics of systems in unknown health state were compared to those corresponding to the (previously modeled) healthy system, and statistical detection of damage and evaluation of its severity was performed. The approach was tested with data obtained from systems in healthy or damaged state. Various levels of damage were simulated by means of holes sequentially drilled onto the slab (one extra hole created at each test). The results were promising since all damaged systems were detected as such and in all but one cases the damage level was correctly assessed.

References

[1] D. Kouzoudis and D.E. Mouzakis, *A 2826 Metglas ribbon as a strain sensor for remote and dynamic mechanical measurements*, Sensors and Actuators A: Physical, 127(2):355--359, 2006.
[2] A. Hernando, M. Vázquez and J.M. Barandiarán, *Metallic glasses and sensing applications*, Journal of Physics E: Scientific Instruments, 21(12):1129--1139, 1988.
[3] E. Hristoforou, *Magnetostrictive delay lines: Engineering theory and sensing applications*, Measurement Science and Technology, 14(2): R15--R47, 2003.
[4] J. Arcas, C. Gómez-Polo, M. Vázquez and A. Hernando, *Sensor applications based on induced magnetic anisotropy in toroidal cores*, Sensors and Actuators A: Physical, 57(1):101--104, 1997.
[5] R. Isermann, *Fault diagnosis of machines via parameter estimation and knowledge processing – Tutorial paper*, Automatica, 29(4):815--835, 1993.
[6] M. Basseville, *Detecting changes in signals and systems: A survey*, Automatica, 24(3):309--326, 1988.
[7] S.D. Fassois and D.G. Dimogianopoulos, *Fault detection and identification in stochastic mechanical systems: An overview with applications*, Proceedings of the 5th National Conference of the Hellenic Society for Non-Destructive Testing "Non-Destructive Testing: Certification, Applications, New Developments", Athens, Greece, 2005.
[8] D.G. Dimogianopoulos, J.D. Hios and S.D. Fassois, *Fault detection and isolation in aircraft systems using stochastic nonlinear modeling of flight data dependencies*, Proceedings of the 14th Mediterranean Conference on Control Automation, MED 2006, Ancona, Italy, 2006.
[9] S.D. Fassois and J.S. Sakellariou, *Time series methods for fault detection and identification in vibrating structures*, Philosophical Transactions of the Royal Society A: Mathematical, Physical and Engineering Sciences, 365(1851): 411--448, 2007.
[10] S. Billings, S. Chen and M. Korenberg, *Identification of MIMO nonlinear systems using a forward-regression orthogonal estimator*, Int. Journal of Control, 49(6):2157--2189, 1989.
[11] S.D. Fassois, *Parametric Identification of Vibrating Structures*, Encyclopedia of Vibrations, Editors: S. Braun, D. Ewins, S. Rao, 2001.
[12] G. Box, G. Jenkins and G. Reinsel, *Time Series Analysis, Forecasting and Control*, Prentice Hall, Englewood Cliffs, NJ, 1994.
[13] T. Söderstrom and P. Stoica, *System Identification*, Prentice Hall-Int, London, 1989.